Fast and Accurate Electric Field Estimation from a Single Ray Tracing Simulation

Juan Pascual-García, José-María Molina-Garcia-Pardo, María-Teresa Martínez-Inglés, José-Víctor Rodríguez, and Leandro Juan-Llácer

Universidad Politécnica de Cartagena (UPCT)
Departamento de Tecnologías de la Información y las Comunicaciones
Antiguo Cuartel de Antigones, Plaza del Hospital, 1, 30202 Cartagena (Murcia), Spain
{juan.pascual, josemaria.molina, mteresa.martinez, jvictor.rodriguez, leandro.juan}@upct.es

Abstract ─ In this work, an efficient field estimation technique is developed. This technique uses a single simulation of a ray tracing tool, at one spatial point at one frequency, to compute the field in the vicinity of the simulated point throughout a complete frequency range. The developed technique is a two-step procedure. Firstly, it operates over the images and field contributions generated by the ray tracing tool at the simulated receiver point to obtain an appropriate set of field contributions for each new receiver point. Secondly, once the new set of images and contributions at one frequency is obtained, a very simple extrapolation procedure is applied to obtain the electric field throughout a frequency range. The whole technique is computationally very efficient and it is also accurate, as the measurements comparison shows.

Index Terms ─ mm-W band, radio channel characterization, ray tracing, wave propagation prediction.

I. INTRODUCTION

Present and future wireless communication systems require accurate and fast radio channel characterization techniques to achieve a successful design and deployment. Ray-optical propagation techniques are one of the most precise approaches to estimate the received electric field in a known environment [1-3]. These techniques include "brute force" ray tracing, also called ray launching, and ray tracing based on image theory.

The main drawback of these techniques is the high computational cost which, consequently, implies a slow channel prediction. Therefore, several efforts have been made to reduce the simulation time. Most of these methods are based on the analysis of the topological relations between the transmitter position, the objects in the environment, and the receiver position. The relations analysis can be used to establish those objects that yield significant propagation paths, reducing in that way the complexity of the field prediction problem. This idea was exploited in [4], where the visibility tree concept was introduced. Subsequently, this concept was improved in other works. In [5], a sweep line algorithm was developed in order to efficiently obtain the visibility tree. In [6], the visibility tree mechanism was improved in order to construct the tree and find the paths at the same time. The main disadvantage of the visibility tree is the dependence on the transmitter and receiver positions. If the receiver changes its position the tree must be recalculated.

Other works used the topological information without applying the visibility tree concept. In [7], the topological information of the environment, which is independent of the transmitter and receiver, was analyzed to compute the relation between walls only once; this information can be used to estimate the wave propagation at different receiver points. A different approach consists of dividing the coverage area into sectors where the visibility conditions are evaluated. This approach was used in [8], where for each source and each receiver a list of visible objects was obtained from the sectors information. Recently, virtual sources (images) were used to define the so-called ray entities in a "brute force" ray tracing tool [9]; one ray entity defines a path where a propagation mechanism is present. The generation of ray entities was used to reduce the memory usage and the computational burden of new ray tracing simulations.

In [10], a spherical wave model was used to obtain the multiple-input and multiple-output (MIMO) channel from a single-input and single-output (SISO) channel. By considering the previous model, a new electric field estimation technique based on 3D ray tracing has been developed in the presented work. Firstly, all images are calculated for one receiver point. Each image represents one ray that reaches the receiver point. The developed technique modifies the module and phase of each ray in order to obtain an appropriate set of rays at a new

Submitted On: February 13, 2014
Accepted On: November 2, 2014

receiver point. Thus, the new technique is able to predict the field at several receivers, whereas the above mentioned works, except [7] and [9], depend on the receiver position. After the calculation of the new rays for each new receiver point, a simple frequency extrapolation technique is applied. Therefore, the whole technique is able to predict the field at a set of points throughout a certain bandwidth from only one simulation at one point at one frequency.

The presented technique has been validated through a comparison with data obtained from measurements in the 60 GHz band. This band has been selected because it is a very promising option for the deployment of future Gbps wireless systems [11]. The design and deployment of these systems needs fast and reliable field prediction techniques and channel estimator tools like the one developed in this work. Moreover, this band represents a difficult test due to the structural complexity of the channel in the mm-W band.

The paper is organized as follows. In Section II the field prediction technique, based on the calculation of a new set of images, is presented. In Section III the frequency extrapolation procedure is shown. Section IV presents the validation of the proposed technique by means of measurements, and finally Section V shows the conclusions.

II. FIELD PREDICTION TECHNIQUE

A. Technique explanation

Ray tracing tools evaluate the total received field considering different field contributions at the receiver point. Specifically, ray tracing based on image theory considers each contribution as a spherical wave that departs from one image and reaches directly the receiver point. Different types of contributions can be considered:

- Line-of-sight ray from the transmitter: in this case the image is the transmitter itself.
- Single reflections: each single reflection is evaluated from the images of the transmitter with respect to the elements of the environment. These images are named first order images.
- Multiple reflections: images of each first order image can be calculated; these second order images represent double reflection contributions. The process of creating new images can be applied successively in order to evaluate the contribution of multiple reflections (M-order reflections).
- Diffracted rays: in this case, the impact point of the wedge where the diffraction takes place must be determined. Uniform theory of diffraction (UTD) is used to evaluate the diffracted field.
- Reflections of a diffracted ray: the above mentioned diffraction point can be considered as a new transmitter. First and higher order images of this point can be calculated to evaluate the field corresponding to these contributions.
- Diffracted rays of a reflected ray: a reflected ray can be diffracted in one wedge. In this case, the diffraction point must be determined taking into account the reflection image position.

In the presented technique, a ray tracing tool is used to obtain the images and field contributions at one point. The ray tracing tool was developed by our research group and considers all previous contributions; in [12], the main characteristics of this tool are briefly explained. The developed ray tracing tool was validated by comparing simulations and measurements of different scenarios found in [13] and [14] with simulations performed using our tool. We call the simulated point the original receiver point. After this first ray tracing calculation, the original images and contributions are transformed in order to evaluate the contributions at a new receiver point placed near the original receiver point. The transformation is based on a module and phase change, as explained below.

Each type of contribution needs a suitable transformation. The original line-of-sight field, assuming spherical wave propagation, is shown in Eq. 1:

$$H_{LOS,O} = \frac{1}{R_{Tx-O}} \cdot e^{-j\vec{k}\cdot\vec{R}_{Tx-O}}, \qquad (1)$$

where k is the wave number and $R_{Tx\text{-}O}$ is the distance between the transmitter and the original receiver point (O), as seen in Fig. 1.

The line-of-sight field at the new receiver point can be straightforwardly evaluated from the original field by applying the transformation shown in Eq. 2:

$$H_{LOS,N} = H_{LOS,O} \cdot e^{-j\vec{k}\cdot(\vec{R}_{Tx-N}-\vec{R}_{Tx-O})} \cdot \frac{R_{Tx-O}}{R_{Tx-N}}, \qquad (2)$$

where $R_{Tx\text{-}N}$ is the distance between the transmitter and the new receiver point (N).

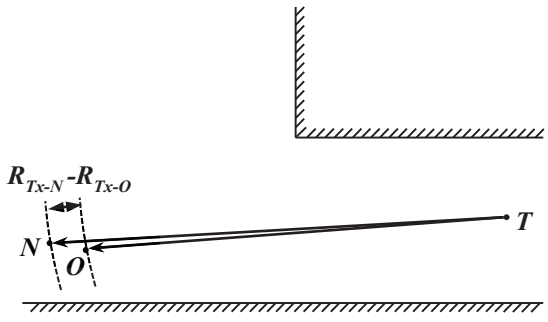

Fig. 1. Line-of-sight scheme. Original receiver point (O), new receiver point (N), and transmitter (Tx) positions are shown. The difference between distances, $R_{Tx\text{-}N}$-$R_{Tx\text{-}O}$, is used to calculate the field at the new receiver point.

The field corresponding to an M-order reflection is

calculated using the M-order image:

$$H_{REFL,O} = \frac{1}{R_{I-O}} \cdot \Gamma \cdot e^{-j\vec{k}\cdot\vec{R}_{I-O}}, \quad (3)$$

where k is the wave number, Γ is the reflection coefficient for single reflections and the accumulated reflection coefficient for multiple reflections [13], and $R_{I\text{-}O}$ is the distance between the M-order image and the original receiver point.

Once the original field is evaluated at the original receiver point, the reflection field at the new receiver point can be estimated by applying the next transformation:

$$H_{REFL,N} = H_{REFL,O} \cdot e^{-j\vec{k}\cdot(\vec{R}_{I-N}-\vec{R}_{I-O})} \cdot \frac{R_{I-O}}{R_{I-N}}, \quad (4)$$

where $R_{I\text{-}N}$ is the distance between the M-order image and the new receiver point. In Fig. 2, the particular situation of M=1, which corresponds to a single reflection ray, is shown; in this case the image is the transmitter image. For M=2, which corresponds to a two-reflection ray, the image used in Eq. 4 to compute the desired field is the image of a first-order image. In this way, Eq. 4 can be applied for any M-order reflection using the appropriate M-order image.

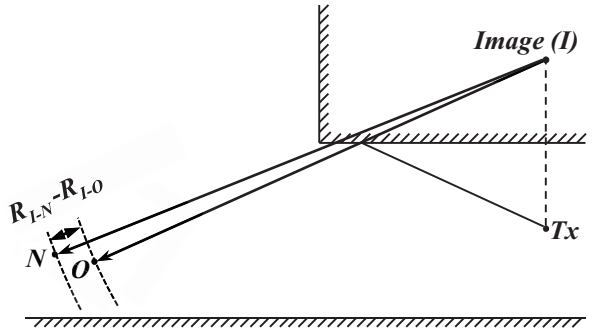

Fig. 2. Single reflection scheme. The difference between distances, $R_{I\text{-}N}$-$R_{I\text{-}O}$, is used to calculate the field at the new receiver point.

It is assumed that the reflection coefficient does not change in a significant way in the vicinity of the original receiver point, this way Γ in Eq. 3 is used in Eq. 4. The area where this approximation is acceptable depends on the diversity of the environment. If the diversity of the environment is high the area will be small; however, even in high diversity scenarios, as the one used in this work to test the developed method, the reflection coefficient remains constant inside an area wide enough to characterize the channel with accuracy.

The field corresponding to a diffracted wave is evaluated using the uniform theory of diffraction (UTD) as seen in Eq. 5:

$$H_{DIF,O} = D\left(\phi_O, \phi_O', L_O, k, \beta_0', n\right) \cdot A\left(s_O, s_O'\right) \cdot \frac{1}{s_O'} \cdot e^{-j\vec{k}\cdot\left(\vec{s}_O+\vec{s}_O'\right)}, \quad (5)$$

where k is the wave number, D is the diffraction coefficient introduced by Luebbers in [15], ϕ_O' is the angle between the transmitter and the "0" face, ϕ_O is the angle between the original receiver point and the "0" face, β_0' is the angle between the transmitter and the edge where the diffraction point is placed, s_O' is the distance between the transmitter and the diffraction point, s_O is the distance between the original receiver point and the diffraction point, and n depends on the angle between the "n" face and the "0" face [14]. All these parameters are depicted in Fig. 3.

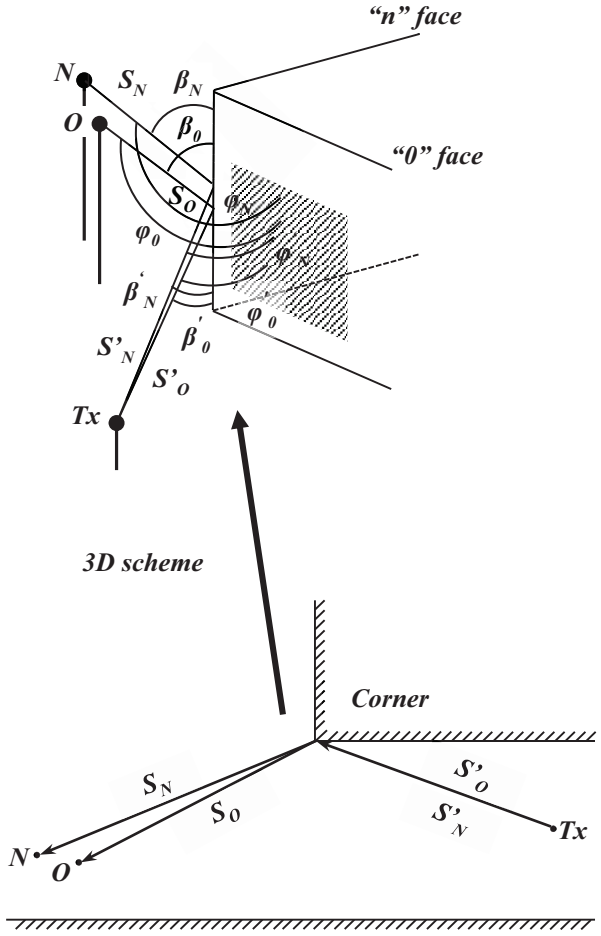

Fig. 3. Diffraction scheme. The diffraction parameters for the original receiver point and for the new receiver point are shown. The new receiver point has its own diffraction impact point in the wedge.

The parameter L_o in Eq. 5 is:

$$L_O = \frac{s_O^{'} s_O \sin^2 \beta_0}{s_O^{'} + s_O}, \tag{6}$$

and the parameter A in Eq. 5 is:

$$A\left(s_O^{'}, s_O\right) = \sqrt{\frac{s_O^{'}}{s_O \cdot \left(s_O^{'} + s_O\right)}}, \tag{7}$$

since the wave is considered to be spherical.

The diffraction field depends on the impact point position as seen in Fig. 3. This impact point depends on the receiver position. Therefore, the modification of the diffracted wave at the new receiver point implies the calculation of a new impact point in the diffraction wedge, as depicted in Fig. 3. New angles $(\phi_N^{'}, \phi_N)$ and distances $(s_N^{'}, s_N)$ must be calculated for the field estimation at the new receiver point. Distance $s_O^{'}$ (s_O) cannot be used in the new field estimation because this distance could be very different to $s_N^{'}$ (s_N) in terms of wavelengths. Thus, the use of $s_O^{'}$ and s_O may yield a large difference in the field phase, which affects the whole field evaluation.

The field at the new receiver point corresponding to the diffracted wave can be expressed as:

$$H_{DIF,N} = D\left(\phi_N, \phi_N^{'}, L_N, k, \beta_N^{'}, n\right) \cdot A\left(s_N, s_N^{'}\right) \cdot \frac{1}{s_N^{'}} \cdot e^{-j\vec{k}\cdot\left(\vec{s}_N + \vec{s}_N^{'}\right)}, \tag{8}$$

where the parameters $(\phi^{'}, \phi, \beta^{'}, s^{'}, s, L)$ have been recalculated for the new receiver point, as seen in Fig. 3.

Single reflections of a diffracted wave are also considered as contributions to the total received field. The field of such contributions can be evaluated as:

$$H_{DIF\_REFL,O} = D\left(\phi_O, \phi_O^{'}, L_O, k, \beta_0^{'}, n\right) \cdot A\left(s_O, s_O^{'}\right) \cdot \frac{1}{s_O^{'}} \cdot \Gamma \cdot e^{-j\vec{k}\cdot\left(\vec{s}_O + \vec{s}_O^{'}\right)}, \tag{9}$$

where the Γ is the reflection coefficient and s_O is now the total distance between the diffraction point and the original receiver point.

As in the previous case, it is necessary to calculate a new diffraction point for each new receiver point. The new diffraction point implies new diffraction parameters as well as a new image, as shown in Fig. 4. Once all the new parameters are recalculated, the field at the new receiver point due to this type of contribution is expressed as follows:

$$H_{DIF\_REFL,N} = D\left(\phi_N, \phi_N^{'}, L_N, k, \beta_N^{'}, n\right) \cdot A\left(s_N, s_N^{'}\right) \cdot \frac{1}{s_N^{'}} \cdot \Gamma \cdot e^{-j\vec{k}\cdot\left(\vec{s}_N + \vec{s}_N^{'}\right)}, \tag{10}$$

where s_N is the total distance between the new diffraction point and the new receiver point, as seen in Fig. 4. It is assumed that the reflection coefficient does not change in a significant way, so Γ in Eq. 10 is the reflection coefficient used in Eq. 9. All the new diffraction parameters are recalculated as in the single diffraction case.

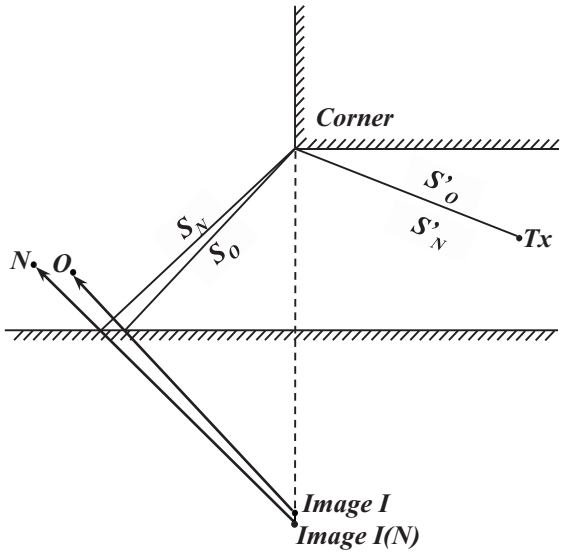

Fig. 4. Diffraction plus reflection scheme. The new receiver point has its own diffraction impact point, which implies a new image called I(N). The image of the original impact point is called image I.

Finally, diffracted rays of reflected rays are considered. In these contributions a single reflection wave impinges in a wedge and suffers a diffraction process before reaching the receiver point. The field corresponding to this type of contributions is:

$$H_{REFL\_DIF,O} = D\left(\phi_O, \phi_O^{'}, L_O, k, \beta_0^{'}, n\right) \cdot A\left(s_O, s_O^{'}\right) \cdot \frac{1}{s_O^{'}} \cdot \Gamma \cdot e^{-j\vec{k}\cdot\left(\vec{s}_O + \vec{s}_O^{'}\right)}, \tag{11}$$

where $s_O^{'}$ is the total distance between the transmitter and the diffraction point. This distance is the distance from the transmitter image I to the diffraction point, as seen in Fig. 5.

In this case, the new field evaluation does not imply a new image calculation as in the diffraction plus reflection case shown in Fig. 5. Nevertheless, it is necessary again to calculate a new impact point of the diffraction wedge. Therefore, new diffraction parameters are evaluated as seen in Eq. 12:

$$H_{REFL\_DIF,N} = D\left(\phi_N, \phi_N^{'}, L_N, k, \beta_N^{'}, n\right) \cdot A\left(s_N, s_N^{'}\right) \cdot \frac{1}{s_N^{'}} \cdot \Gamma \cdot e^{-j\vec{k}\cdot\left(\vec{s}_N + \vec{s}_N^{'}\right)}, \tag{12}$$

where $s_N^{'}$ is the total distance between the transmitter and the new diffraction point as seen in Fig. 5.

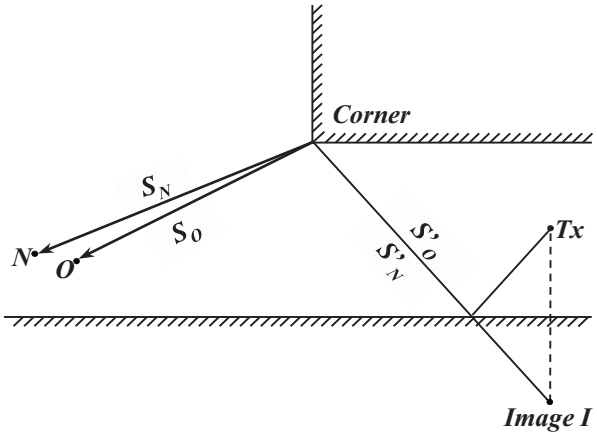

Fig. 5. Reflection plus diffraction scheme. The new receiver point has its own diffraction impact point.

B. Technique validation through simulations

The precision of the described field prediction technique has been checked in two ways. Firstly, the technique results have been compared with simulation results obtained from the ray tracing tool. Secondly, the usefulness of the technique has been tested by means of a comparison with results extracted from measurements. In this section we show the comparison with ray tracing simulations, and in Section IV we show the measurements comparison.

The measurement (and simulated) scenario, which is shown in Fig. 6, is a laboratory located on the first floor of the Universidad Politécnica de Cartagena research building (Spain). The 4.5 × 7 × 2.5 m laboratory is furnished with several cupboards, shelves, desktops, and chairs as seen in Fig. 6. A numerical model of the scenario has been generated in order to estimate the field with the ray tracing tool and with the developed field prediction technique. As seen in Fig. 7, the mentioned numerical model is a satisfactory representation of the measured scenario as it includes the main scenario elements.

Fig. 6. Photo of the measured scenario.

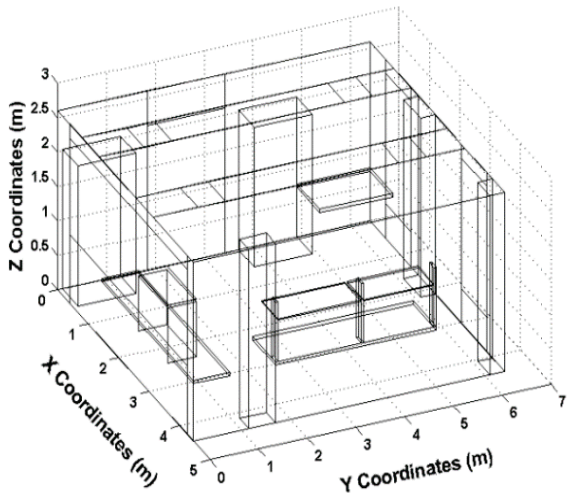

Fig. 7. Modeled scenario of Fig. 6.

Two sets of receiver positions (Rx_1 and Rx_2) and one set of transmitter positions (Tx) have been used to test the prediction technique. Each receiver set is composed of 36 positions distributed in a regular grid, as depicted in Fig. 8. The separation between two consecutive positions is 2 mm; this distance is lower than λ/2, with λ=5 mm at the central frequency of the band. Thus, the total coverage of the regular grid is 1 cm × 1 cm. As seen in Fig. 8, the transmitter set is composed of 5 positions; the separation between two consecutive transmitter positions is also 2 mm. The height of the transmitter positions is 1.44 m and the height of the receiver positions is 1.54 m.

Thus, the field was simulated with the ray tracing tool in the 36 regular grid distributed positions of Rx_1 and Rx_2. The developed technique was also used to evaluate the field at the mentioned positions from a single simulation; in each set, the single simulation was performed at a point placed in the central position of the corresponding regular grid; this point is the original receiver point of Eq. 1-12. In this section, the Tx point is the third position of the linear array scheme shown in Fig. 8.

Different contributions were considered in the field simulation: single and second order reflections, diffracted waves, reflected waves from diffracted waves, and diffracted waves from the single reflected waves. Furthermore, real omnidirectional antenna patterns were included in the simulation in order to represent faithfully the performed measurements shown in Section IV. In Fig. 9 (a) and Fig. 10 (a), the channel attenuation at 61.5 GHz estimated with the ray tracing tool is shown for Rx_1 and Rx_2, respectively. The difference between the attenuation computed with the ray tracing tool and the field prediction technique is depicted in Fig. 9 (b) and Fig. 10 (b). Both figures show the high accuracy reached by the field prediction technique; the maximum error in

the Rx_1 set is below 0.03 dB and in the Rx_2 case is also very small (0.43 dB).

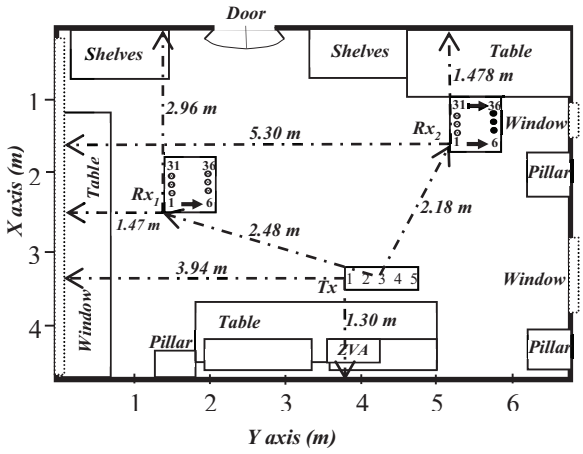

Fig. 8. Scheme of the measured and simulated positions.

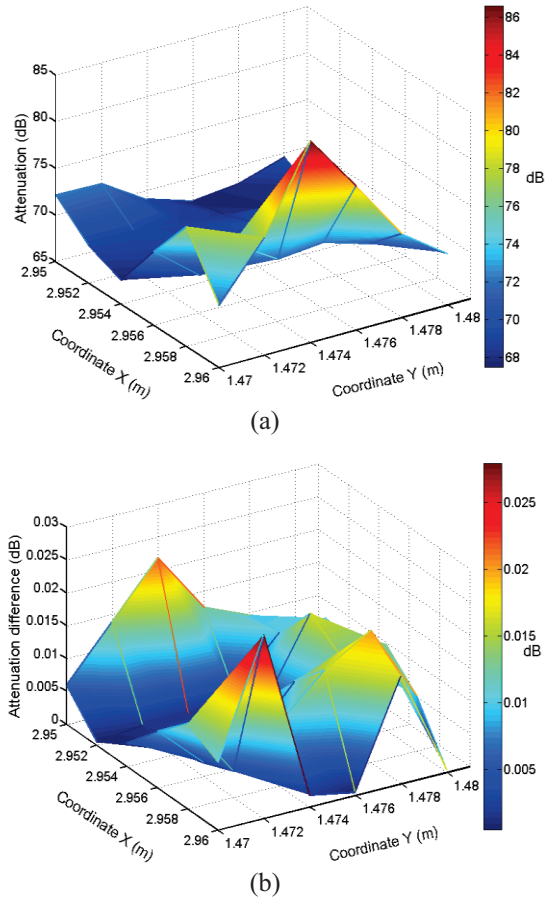

Fig. 9. (a) Attenuation at 61.5 GHz for Rx_1 positions, and (b) attenuation difference between the ray tracing tool and the presented field prediction technique.

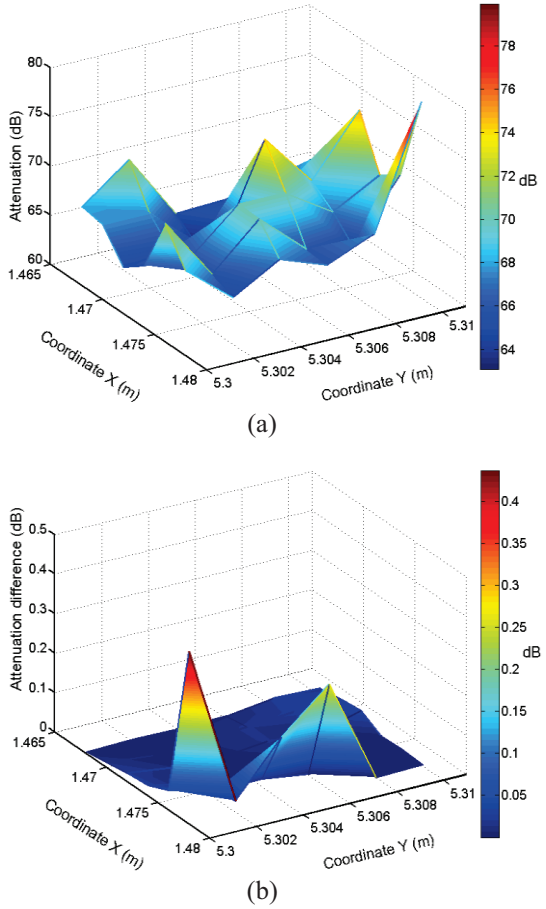

Fig. 10. (a) Attenuation at 61.5 GHz for Rx_2 positions, and (b) attenuation difference between the ray tracing tool and the presented field prediction technique.

The presented technique is very accurate in the field evaluation of all contributions. The normalized mean square error (NMSE) between the simulated and predicted field values has been used to compare the precision of the new technique in all propagation mechanisms considered. The NMSE of a given propagation mechanism is defined as:

$$NMSE = \sqrt{\frac{\sum_{i=1}^{P}\left|H_{sim,i} - H_{pred,i}\right|^2}{\sum_{i=1}^{P}\left|H_{sim,i} - \bar{H}_{sim}\right|^2}}, \qquad (13)$$

where P is the number of points in the receiver set (P=36), $H_{sim,i}$ is the total electric field corresponding to a propagation mechanism simulated with the ray tracing technique in the *i-th* spatial point, $\bar{H}_{sim}$ is the mean of the P values, and $H_{pred,i}$ is the total electric field corresponding to the same propagation mechanism predicted with the developed technique at the *i-th* spatial

point.

In Table 1, the NMSE of the propagation mechanisms corresponding to positions sets Rx_1 and Rx_2 is shown. The wavelength at 60 GHz is very small; thus, any error in the phase transformation or any incorrect new image calculation would yield large NMSE levels. Nevertheless, the computed NMSE is very low for all types of propagation mechanisms, even for the Diffr_Refl mechanism in Rx_2. Therefore, the presented technique will be accurate regardless of the predominant propagation mechanism, provided that the original and the new receiver points have the same contributions.

The main advantage of the field prediction technique is the time saved in the computation of the desired channel response. The simulation of 36 positions takes 1000 seconds; the new technique needs only one simulation (less than 30 seconds) and 75 seconds for the computation of the field at the P=36 receiver points. Thus, in this example, the field prediction technique is approximately 10 times faster than the ray tracing tool. Moreover, as the number of simulated positions increases, the new technique becomes more profitable. All simulations were performed with a computer based on a 64 bits Intel CPU at 3.20 GHz with 8 GB RAM.

Table 1: NMSE for all considered propagation mechanisms. Refl corresponds to reflected waves, Diffr corresponds to diffracted waves, Diffr_Refl corresponds to waves reflected after diffraction, and Refl_Diffr corresponds to waves diffracted after a reflection

Set	Refl	Diffr	Diffr_Refl	Refl_Diffr
Rx_1	0.00630	0.00100	0.00730	0.00020
Rx_2	0.00030	0.00020	0.06480	0.00002

III. FREQUENCY EXTRAPOLATION PROCEDURE

A. Frequency extrapolation procedure explanation

The field prediction technique explained above is able to evaluate the field in the vicinity of a given point at one frequency. Therefore, the prediction technique is limited to one frequency evaluation, which could make the technique impractical, especially if the frequency channel response evaluation is desired. For this reason, we have applied a very simple extrapolation procedure to evaluate the field in a given frequency range from the contributions at one frequency. The mentioned procedure consists of the phase correction in every contribution. The field of one contribution can be expressed as:

$$H_1 = |H_1| \cdot e^{j\phi_1} \cdot e^{-j\vec{k}_1 \cdot \vec{R}}, \quad (14)$$

where R is the total distance traveled by the wave, k_1 is the wave number at frequency f_1, and ϕ_1 is a term which depends on the reflection coefficients, diffraction coefficients, and the antenna pattern.

We assume that, for all frequencies in the frequency range, the reflection and diffraction coefficients remain constant. This assumption is feasible even for large bandwidths because the electromagnetic properties of the materials remain constant in large bandwidths [13]. Thus, the extrapolation procedure performs a phase correction only in the term which depends on the distance:

$$H_2 = H_1 \cdot \frac{e^{-j\vec{k}_2 \cdot \vec{R}}}{e^{-j\vec{k}_1 \cdot \vec{R}}} \cdot \quad (15)$$

The above equation yields the extrapolated field in frequency f_2 from the known field in frequency f_1.

The complete technique follows the next steps:

1. Obtain the contributions and images at one point (original receiver point) with the ray tracing tool at one frequency.
2. Apply the field prediction technique explained in Section II at a new receiver point at the mentioned frequency. This step gives a suitable set of contributions for the new receiver point.
3. Apply the frequency extrapolation procedure to every contribution calculated in the previous step. This procedure yields a set of contributions at a new frequency for the new receiver point.

B. Frequency extrapolation procedure validation through simulations

In order to test the frequency extrapolation procedure, the frequency response in the 60 GHz band was calculated with the ray tracing tool and with the prediction technique. The number of frequency points was set to 4096 and the bandwidth ranges from 57 GHz to 66 GHz. The prediction technique uses the 61.5 GHz frequency to evaluate the original received field. In Fig. 11 (a), the difference between both frequency responses is shown for one point selected from the Rx_1 set; the selected point corresponds to the one where the error performed with the prediction technique was largest at 61.5 GHz. In Fig. 11 (b), the same comparison is depicted for the worst point of the Rx_2 set. Both figures show the high accuracy of the complete technique, which involves the prediction of the field at a new spatial point and the frequency extrapolation. In both cases, the transmitter point is the third position of the linear set shown in Fig. 8.

The precision of the new technique is clearly shown when the complex impulse response h(τ) (CIR) is calculated. The channel is static; therefore the CIR can be evaluated from the frequency response by applying an inverse Fourier transform:

$$h(\tau) = FT^{-1}\{H(f)\}. \quad (16)$$

In Fig. 12 (a) and Fig. 12 (b) the absolute value, expressed in logarithmic units, of the CIR evaluated with the two techniques is depicted. In Table 2, the root mean square delay spread (RMS DS) and the path loss (PL) are

shown for the studied CIR. A 30 dB threshold was used in the RMS delay spread calculation to keep the most energetic paths. The agreement between the original ray tracing and the complete technique is excellent, as seen in Fig. 12 and in Table 2.

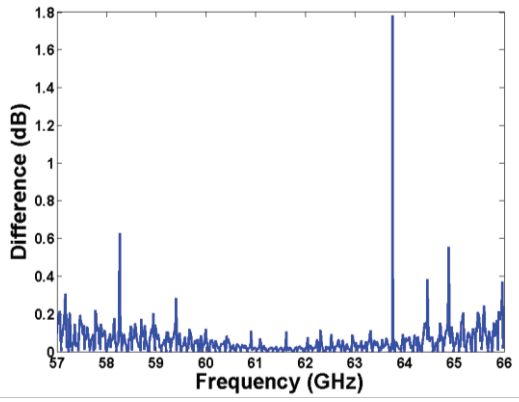

(a)

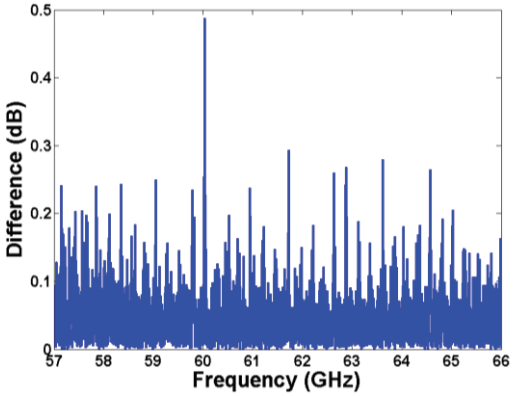

(b)

Fig. 11. Difference in dB between the frequency responses calculated with the ray tracing tool and the developed technique. In (a), the difference corresponding to the worst point of Rx_1 is shown; in (b), the difference corresponding to the worst point of Rx_2 is shown.

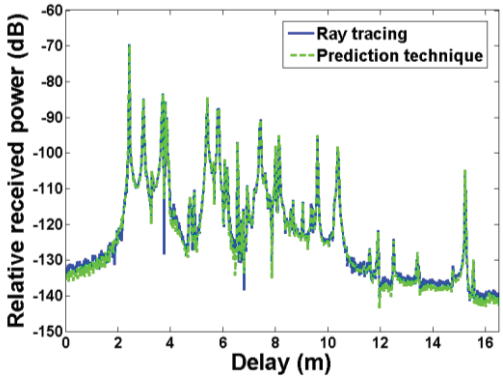

(a)

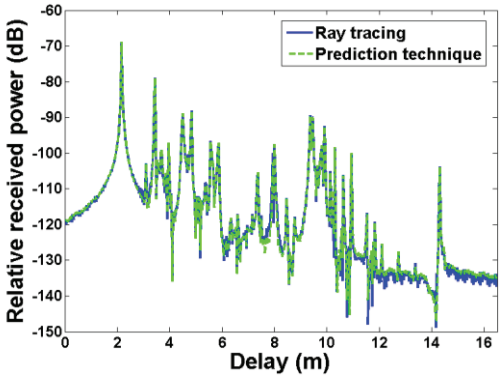

(b)

Fig. 12. CIR calculated with the ray tracing tool and the developed technique. In (a), the CIR of the worst point of Rx_1 is depicted; in (b), the CIR of the worst point of Rx_2 is depicted.

Table 2: RMS delay spread and path loss of the CIR shown in Fig. 12, which correspond to the worst points of the studied sets. These parameters have been evaluated for the new prediction technique data and for the original ray tracing tool (RT) data

Position	RMS DS (ns)		PL (dB)	
	RT	Prediction	RT	Prediction
Rx_1	3.52	3.52	68.62	68.62
Rx_2	4.22	4.17	67.75	67.74

IV. VALIDATION BASED ON MEASUREMENTS

The complete technique explained in Sections II and III was tested through measurements performed in the laboratory shown in Fig. 6. In particular, the frequency response was measured for every pair of transmitter and receiver positions depicted in Fig. 8. The channel sounder is based on a Rohde & Schwartz ZVA67 Vector Network Analyzer (VNA). As in the simulations of Section III, the measured frequency range was 57–66 GHz using 4096 frequency points. A 10 Hz intermediate frequency was selected and a dynamic range of more than 100 dB was obtained. Two amplifiers were used in the transmission to compensate for the attenuation of the used cables (HXI HLNA-465). The system is through calibrated to eliminate the effect of cables and amplifiers. The VNA Tx power was set to -10 dBm.

Both Tx and Rx antennas are vertically-polarized omnidirectional antennas (Q-par QOM55-65 VRA) with 4.5 dBi gain. As in the simulations of the previous section, the height of the transmitting antenna was 1.44 m and 1.54 m for the receiving antenna. Nobody was inside the room during the measurements campaign, so the channel can be considered as static.

Once all frequency responses were collected, the CIR for every pair of points was calculated by applying the inverse Fourier transform operation shown in Eq. 16.

The power delay profile (PDP) of each one of the two Tx-Rx sets is the ensemble of the corresponding complex impulse responses [13]:

$$PDP(\tau) = \left\langle |h(\tau)|^2 \right\rangle . \quad (17)$$

The PDP of the Tx-Rx sets was also evaluated with the field prediction technique. For each one of the five Tx positions a single simulation with the ray tracing tool was performed. This simulation allowed the calculation of the field corresponding to all propagation mechanisms, at all Rx set points at the central frequency 61.5 GHz. The frequency extrapolation procedure was then applied in order to obtain the frequency response at all points. Therefore, the PDP evaluation with the new technique needed:

1. The calculation of five simulations with the ray tracing tool (see Table 3).
2. Five executions of the spatial field prediction technique explained in Section II. This technique is at least one order of magnitude faster than the ray tracing simulations.
3. The execution of the frequency extrapolation at each one of the Rx points for each one of the Tx positions. A total of 36•5=180 executions of this procedure are needed. Each execution is very fast as it needs only 0.85 seconds to evaluate the frequency response for one spatial point.

The time taken by the new technique is very small in comparison with the time needed by the ray tracing tool as seen in Table 3. The new technique takes only 668 seconds to evaluate the PDP for each Rx set, whereas the ray tracing tool would have needed a huge amount of time (the time shown in Table 3 for the ray tracing tool is an estimation based on the time needed to compute one CIR). The measurements also needed several days to be completed, as seen in Table 3. Thus, the new technique is a very useful tool to characterize the wireless channel.

Table 3: Time taken to calculate the PDP with the new technique, time theoretically needed to compute the PDP with the original ray tracing tool, and time spent to measure the channel. All simulations were performed with a computer based on a 64 bits Intel CPU at 3.20 GHz with 8 GB RAM

New Technique			
5 Simulations with the RT	5 Executions of Spatial Field Prediction	5x36 = 180 Executions of Frequency Extrapolation	Total Time
140 s.	375 s.	153 s.	668 s.
Ray Tracing Tool			
5x36x4096 = 737280 simulations with the RT			
>238 days			
Measurement Time			
3 days			

The precision of the new technique can be perceived in Fig. 13. The new technique is able to properly grasp the main propagation mechanisms. For the sake of comparison, noise was added to the simulated CIR.

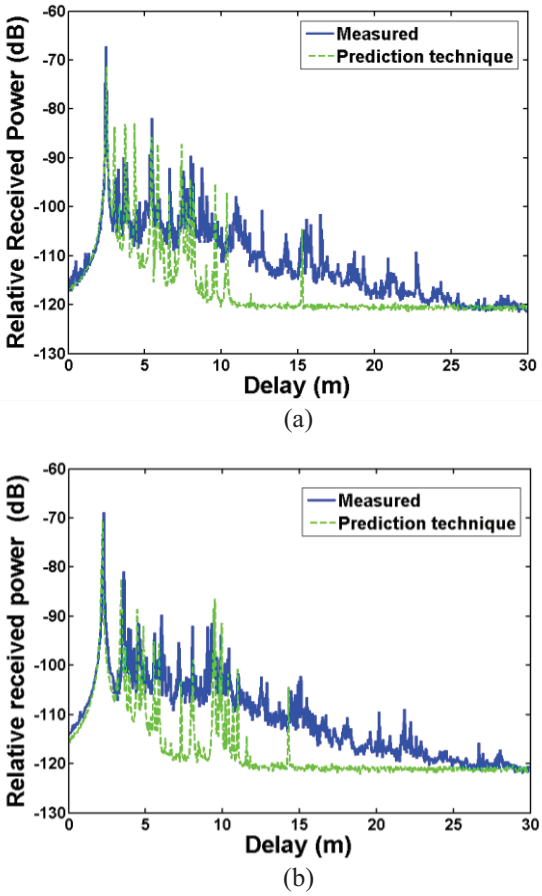

Fig. 13. (a) PDP of the Rx_1 set, and (b) PDP of the Rx_2 set. The measured PDP and the PDP obtained through the prediction technique are compared.

The accuracy of the new technique has also been quantitatively tested. Table 4 summarizes the RMS delay spread and path loss of the PDPs. As in Section III, a 30 dB threshold was used in the RMS delay spread calculation. As seen in Table 4, the new technique is a reliable tool to characterize the wireless channel, even in the complex 60 GHz band. Some differences are found in Table 4, i.e., in the PL of Rx_2; however, such differences are, in part, attributable to the imperfect representation of both the antenna patterns and the modeling of the scenario.

The PDP in this work was evaluated in an area of 1 cm × 1 cm. As the frequency decreases the area needed to evaluate the PDP increases. Therefore, one original receiver point might not be enough to obtain accurate results. In this case, new original receiver points can be simulated increasing the accuracy; the proposed

technique would be still profitable since the time saved is very large as seen in Table 3.

Table 4: RMS delay spread and Path Loss of the PDP shown in Fig. 13. These parameters have been evaluated for the new prediction technique data (Pred.) and for the measured data (Meas.)

Position Set	RMS DS (ns)		PL (dB)	
	Meas.	Pred.	Meas.	Pred.
Rx_1	3.17	3.98	67.64	68.69
Rx_2	4.35	4.49	64.50	67.98

V. CONCLUSION

A very efficient field prediction technique has been presented. The new technique firstly evaluates the field contributions in the vicinity of one point and secondly performs a frequency extrapolation to yield the frequency response at all new spatial points. The validation results have shown that the precision of the new technique is similar to that obtained with the ray tracing tool, even at high frequencies where the wavelength is very small. Such precision is only reached in the vicinity of the simulated point. Nevertheless, this spatial limitation is enough to calculate channel functions such as the power delay profile. The spatial and frequency limits where the proposed method is accurate will be studied in future works. The presented technique is very fast in comparison with both measurements and ray tracing simulations. Therefore, for all the above reasons, the new technique permits a fast and reliable characterization of the channel. The mentioned ability makes the developed technique a useful tool in the design of wireless communications systems, especially in those that use MIMO techniques and those based on ultrawideband technology.

ACKNOWLEDGMENT

This work was supported by the Ministerio de Economía y Competitividad (MINECO), Spain (TEC2013-47360-C3-2) and by the European FEDER funds.

REFERENCES

[1] G. de la Roche, A. Alayón-Glazunov, and B. Allen, "*Simulation and Performance*," in *LTE-Advanced and Next Generation Wireless Networks: Channel Modelling and Propagation*, John Wiley and Sons, Chichester, UK, pp. 271-292, 2013.

[2] R. A. Valenzuela, "A ray tracing approach to predicting indoor wireless transmission," in *Proc. of IEEE 43rd Vehicular Technology Conference*, pp. 214-218, 1993.

[3] D. Dardari, L. Minelli, V. Tralli, and O. Andrisano, "Fast ray-tracing characterisation of indoor propagation channels at 60 GHz," in *Proc. of IEEE 47th Vehicular Technology Conference*, vol. 2, pp. 989-993, 1997.

[4] M. G. Sánchez, L. de Haro, A. G. Pino, and M. Calvo, "Exhaustive ray tracing algorithm for microcellular propagation prediction models," *Electronics Letters*, vol. 32, no. 7, pp. 624-625, Feb. 1996.

[5] F. Aguado-Agelet, F. Pérez-Fontán, and A. Formella, "Fast ray tracing for microcellular and indoor environments," *IEEE Trans. on Magnetics*, vol. 33, no. 2, pp. 1484-1487, Mar. 1997.

[6] P. Wang, L. X. Guo, and Y. S. Feng, "A fast ray-tracing algorithm for microcellular propagation prediction models," in *Proc. of 10th International Symposium on Antennas, Propagation & EM Theory (ISAPE)*, pp. 436-339, 2012.

[7] A. Toscano, F. Bilotti, and L. Vegni, "Fast ray-tracing technique for electromagnetic field prediction in mobile communications," *IEEE Trans. on Magnetics*, vol. 39, no. 3, pp. 1238-1241, May 2003.

[8] W. M. O'Brien, E. M. Kenny, and P. J. Cullen, "An efficient implementation of a three-dimensional microcell propagation tool for indoor and outdoor urban environments," *IEEE Trans. on Vehicular Technology*, vol. 49, no. 2, pp. 622-630, Mar. 2000.

[9] N. Magata, R. Zentner, and A. Katalanic-Mucalo, "Ray entity based post processing of ray tracing data for continuous modeling of radio channel," in *Proc. of Euro-COST Conference*, 2013.

[10] J. M. Molina-García-Pardo, J. V. Rodriguez, and Leandro Juan-Llacer, "Parametric spherical-wave MIMO model for ray-based simulations," *Radio Science*, Jan. 2007.

[11] P. Smulders, "Exploiting the 60 GHz band for local wireless multimedia access: prospects and future directions," *IEEE Communications Magazine*, vol. 40, no. 1, pp. 140-147, Jan. 2002.

[12] M. T. Martínez-Inglés, J. Pascual-García, J. V. Rodriguez, J. M. Molina-García-Pardo, Leandro Juan-Llacer, D. P. Gaillot, M. Lienard, and P. Degauque, "Indoor radio channel characterization at 60 GHz," in *Proc. of 7th European Conference on Antennas and Propagation (EuCAP)*, pp. 2796-2799, 2013.

[13] T. S. Rappaport, *Wireless Communications: Principles and Practice*, Prentice-Hall, New Jersey, 1996.

[14] A. S. Balanis, *Geometrical Theory of Diffraction, in Advanced Engineering Electromagnetics*, John Wiley and Sons, New York, 1989.

[15] R. Luebbers, "Finite conductivity uniform GTD versus knife edge diffraction in prediction of propagation path loss," *IEEE Trans. on Antennas and Propagation*, vol. 32, no. 1, pp. 70-76, Jan. 1984.

Juan Pascual García was born in Castellón, Spain, in 1975. He received the Telecommunications Engineer degree from the Technical University of Valencia (UPV), Valencia, Spain, in 2001 and the Ph.D. in Communications Engineering from the Universidad Politécnica de Cartagena (UPCT), Cartagena, Spain, in 2010. In 2003, he joined the Communications and Information Technologies Department, UPCT as a Research Assistant and then as an Associated Professor. In 2009 he joined the SiCoMo Research Group of the UPCT where he is currently developing his research tasks.

His research interests include radio wave propagation, ray tracing techniques and radio channel propagation models

José-María Molina-García-Pardo received the Engineer of Telecommunications degree from the Universidad Politécnica de Valencia (Spain, 2000), and the M.Sc. in "Communication and Signal Processing" in Newcastle Upon Tyne (United Kingdom) in September 2001 and the Ph.D. degree in Telecommunications from the Universidad Politécnica de Cartagena (UPCT, Spain) in 2004. In 2001, he joined the Information Technologies and Communications Department of the Universidad Politécnica de Cartagena, where he has been an Associate Professor since 2007, and recently accredited as a Full Professor.

His research activities are centered on radio-communications, propagation, channel modelling and experimental channel sounding in different frequency band (400 MHz to 60 GHz) and technologies (GSM, UMTS, LTE, WiFi, WSN, TETRA, mmW, OFDM, MIMO, cognitive radio). He currently leads the SICOMO research group. He is the Lead Researcher in some national projects, and participates actively in the European COST action IC-1004 (Radio Communications for Green Smart Environments). He is author of more than 50 journals indexed in the JCR, more than 100 international conferences and author of three book chapters.

María-Teresa Martínez-Inglés was born in Sucina, Murcia, Spain, in 1983. She received the Telecommunications Engineering degree in 2009, and the Ph.D. degree in Telecommunications in 2014 from the Universidad Politécnica de Cartagena (UPCT), Cartagena, Spain.

Her research line aims to study the modelling and characterization of the millimeter wave frequency band.

José-Víctor Rodríguez was born in Murcia, Spain, in 1975. He received the Telecommunications Engineering degree from the Universidad Politécnica de Valencia (UPV), Spain, in 2001 - after doing his graduate thesis at the Lund Institute of Technology, Lund University, Sweden, in collaboration with Ericsson Mobile Communications AB - and the Ph.D. in Communications Engineering from the Universidad Politécnica de Cartagena (UPCT), Spain, in 2006. In 2002, he joined the Department of Information Technologies and Communications, at the Universidad Politécnica de Cartagena (UPCT), Spain, where he is currently an Associated Professor.

His research interests include the modeling of radio wave propagation in the mobile environment, with an emphasis on multiple-building diffraction.

Leandro Juan-Llácer was born in Albatera, Alicante, Spain, in 1967. He received the Telecommunications Engineering degree from the Universitat Politècnica de Catalunya (UPC), Barcelona, Spain, in 1993, and the Ph.D. in Communications Engineering from the Universidad Politécnica de Valencia (UPV), Valencia, Spain, in 1998. In 1994, he joined the UPV's Department of Signal Theory and Communications, where he was an Associate Professor (AP) of Electromagnetics from 1995 to 2000. He is currently Professor at the Universidad Politécnica de Cartagena (UPCT)'s Department of Information Technologies and Communications.

He has also been participating in COST actions 256, 259 and 273 and in IC1004 action. His research activities have focused on the characterization and modelling of radio wave propagation in mobile communication systems.